Biogenesis of NDUFS3-less complex I indicates TMEM126A/OPA7 as an assembly factor of the ND4-module

Luigi D'Angelo,[1*] Elisa Astro,[1*] Monica De Luise,[2] Ivana Kurelac,[2] Nikkitha Umesh-Ganesh,[2] Shujing Ding,[3] Ian M. Fearnley,[3] Massimo Zeviani,[3,4] Giuseppe Gasparre,[2,5] Anna Maria Porcelli,[1,6#] Erika Fernandez-Vizarra,[3,7#] and Luisa Iommarini[1#]

[1]Department of Pharmacy and Biotechnology (FABIT), University of Bologna, Bologna, Italy

[2]Department of Medical and Surgical Sciences (DIMEC), University of Bologna, Bologna, Italy

[3]Medical Research Council-Mitochondrial Biology Unit, University of Cambridge, Cambridge, UK

[4]Venetian Institute of Molecular Medicine, Via Orus 2, 35128 Padova, Italy; Department of Neurosciences, University of Padova, via Giustiniani 2, 35128 Padova, Italy

[5]Center for Applied Biomedical Research (CRBA), University of Bologna, Bologna, Italy

[6]Interdepartmental Center of Industrial Research (CIRI) Life Science and Health Technologies, University of Bologna, Ozzano dell'Emilia, Italy

[7]Institute of Molecular, Cell and Systems Biology, University of Glasgow, Glasgow, UK.

*Co-first authors

[#]Co-last authors

To whom correspondence should be addressed:
Luisa Iommarini
Department of Pharmacy and Biotechnology (FABIT)
University of Bologna
Via Francesco Selmi 3, 40126
Bologna, Italy
Tel. +39 051 2091282
e-mail luisa.iommarini2@unibo.it

Erika Fernandez-Vizarra
Institute of Molecular, Cell and Systems Biology
University of Glasgow
University Avenue
Glasgow G12 8QQ, UK
Tel. +44 141 330 6235
e-mail Erika.Fernandez-Vizarra@glasgow.ac.uk

ABSTRACT

Complex I (CI) is the largest enzyme of the mitochondrial respiratory chain and its defects constitute the principal cause of mitochondrial disease. To understand the mechanisms regulating the extremely intricate biogenesis of this fundamental bioenergetic machine, we dissected the structural and functional consequences of the depletion of NDUFS3, a non-catalytic core subunit. We prove that in diverse cell contexts a small, but still detectable, proportion of functional CI can still be found in the absence of NDUFS3. In addition, we have determined the dynamics of disassembly of CI when the amounts of NDUFS3 are gradually decreased. The process of degradation of the complex occurs in a hierarchical and modular fashion where the ND4-module remains stable and bound to TMEM126A. We have thus, uncovered the function of TMEM126A, the product of a disease gene causing optic atrophy, as a factor necessary for the correct assembly and function of CI.

Keywords

Respiratory complex I, CI, NDUFS3, assembly factor, TMEM126A, SILAC

Introduction

Human complex I (CI), NADH: ubiquinone oxidoreductase, is the largest multi-heteromeric enzyme of the mitochondrial respiratory chain (MRC), being composed of forty-five subunits encoded by both the nuclear (nDNA) and the mitochondrial DNA (mtDNA) (1, 2). This enzyme couples the transfer of two electrons from NADH to ubiquinone (coenzyme Q or CoQ) with the pumping of four protons from the matrix to the intermembrane space, contributing to the generation of the proton-motive force necessary for ATP synthesis (1, 2). The essential catalytic core of the enzyme is constituted by the fourteen so-called 'core subunits' evolutionarily conserved from bacteria to the mitochondria of higher eukaryotes (3–5). The remaining thirty supernumerary subunits lack direct catalytic function but are essential for the stability and the biogenesis of the enzyme (6). Supernumerary subunits are entirely nDNA-encoded, while seven core subunits (MT-ND1-6 and MT-ND4L) are encoded by mtDNA (4, 7). This gigantic complex has a distinctive L-shaped structure with a hydrophilic arm protruding into the matrix and a hydrophobic arm embedded in the inner mitochondrial membrane. It can be divided into three main functional modules: NADH dehydrogenase module (N-module), ubiquinone-binding module (Q-module), and proton translocating module (P-module), located entirely in the membrane arm (2). In particular, the transmembrane P-module contains all the mtDNA-encoded subunits and can be further divided into two proximal modules (ND1- and ND2-module) plus two distal modules (ND4- and ND5-module) (6, 8, 9). Such modular organization reflects the enzyme evolution (10, 11), structure (5) and function (1), as well as the pathways involved in its assembly (8). CI biogenesis is an intricate process that takes place in a modular fashion, where each of the functional submodules are assembled and stabilized assisted by a number of specific 'assembly factors', which can be chaperones or proteins involved in prosthetic group incorporation or post-translational modification of the subunits (12). Each of the modules are joined together in different stages forming assembly intermediates, all eventually coming together at the end of the process to form the mature holoenzyme when assembly factors are released (8, 9). To further complicate this scenario, the

practical totality of CI is found associated with complexes III (CIII) and IV (CIV), forming the respiratory supercomplexes (SCs) or 'respirasomes' (13–15). In this context, the biogenesis of CI has been envisioned as either being completed before interacting with CIII and CIV (8, 16), or occurring in the context of the SCs (17, 18).

During CI assembly, the core subunit NDUFS3 has been shown to be part of a subcomplex of about 89kDa containing NDUFS2 and NDUFA5 that appears in the early stages and represents the primary core for the generation of the Q-module (19, 20, 8). Hence, although it lacks a direct catalytic role, NDUFS3 is extremely conserved and seminal for CI assembly, and missense mutations in *NDUFS3* gene are pathogenic for severe neurological conditions such as Leigh Syndrome (LS) (21–23) or encephalomyopathy (24). In addition, a recently developed conditional knock-out (KO) mouse model showed that the ablation of *Ndufs3* in skeletal muscle produced severe progressive myopathy and early mortality (25).

Despite the great advances in the understanding of mammalian MRC biogenesis in general, and in the assembly of CI in particular, there are still many open questions concerning the hierarchy of the different components of these pathways. These questions are relevant not only to understand basic mitochondrial biology, but also the pathological mechanisms underlying disease as CI deficiency is the most frequent biochemical defect causing mitochondrial disorders in humans.

We have previously generated and performed a basic biochemical characterization of two different human cell lines in which the *NDUFS3* gene was knocked-out to study the impact of CI deficiency on tumor progression (26). In the present work, we have further elucidated the role of the non-catalytic but still essential NDUFS3 subunit in CI assembly, stability and function. Our results show that transient or stable ablation of this subunit severely affects the stability of CI, but yet a small fraction of the enzyme is still able to assemble, conserving its NADH:ubiquinone oxidoreductase activity. In addition, we have defined the dynamics of CI disassembly upon the gradual repression of NDUFS3, showing that the distal P-modules containing MT-ND4 and MT-ND5 remain stable,

while all the others are disassembled. Finally, we have identified TMEM126A/Opa7, whose function was thus far unknown, as a CI assembly factor.

Results

A residual fully assembled and functional respiratory CI is present upon *NDUFS3* ablation

We have previously reported that the genetic ablation of *NDUFS3* in two human cell lines, osteosarcoma 143B$^{-/-}$ and colorectal carcinoma HCT116$^{-/-}$, induced a severe decrease of CI NADH dehydrogenase activity and of CI-driven ATP production (Kurelac et al., 2019). However, CI (rotenone-sensitive) activity was not completely absent despite the complete lack of NDUFS3 protein expression in 143B$^{-/-}$ and HCT116$^{-/-}$ (Supplementary Fig. 1A-B, Fig.1A; 13.62% and 20.31% of their relative isogenic controls, respectively). Such residual CI activity was evident also in In-Gel Activity (CI-IGA) at the level of fully assembled CI and supercomplexes (SCs) in both NDUFS3-null models (Fig. 1B-C and Supplementary Fig. 1C-D). The residual activity found in 143B$^{-/-}$ was not detectable in nDNA isogenic cybrids carrying the homoplasmic frameshift mutation m.3571insC/*MT-ND1* (OS) and mtDNA-depleted 143B Rho^{0} cells (Iommarini et al., 2018) (Fig. 1B). Moreover, it was completely abolished by blocking mitochondrial translation with 50 µg/mL chloramphenicol (CAP) (Supplementary Fig. 1E), indicating that the presence of a residual fully assembled and active CI persists despite the lack of NDUFS3. Moreover, CI-IGA was detectable in OS-93 cells in which 7% of wild type *MT-ND1* was able to rescue partially the disassembly of CI, indicating a high sensitivity of the method (Fig. 1B; (27)). *NDUFS3* ablation was accompanied by a severe reduction of several CI subunits belonging to all the structural modules of the enzyme, whereas subunits belonging to CIII and CIV were not affected (Fig. 1D and Supplementary Fig. 1F). Such reduction of CI subunits was associated with the accumulation of subassembled species with positive signal for NDUFB6, NDUFB8 and NDUFA9. Nonetheless, 2D-PAGE confirmed the presence of a residual fully assembled CI in the SCs of 143B$^{-/-}$ and HCT116$^{-/-}$ cells (Fig. 1E and Supplementary Fig. 1G). On the other hand, SC $CIII_2$+IV and fully assembled CIII and CIV were neither structurally affected nor showed defects in their redox activity (Fig. 1E, Supplementary Fig.

1G and Supplementary Fig. 2A-B). Moreover, CS activity was not affected by the lack of NDUFS3 (Supplementary Fig. 2A). We have previously shown that a residual rotenone-sensitive CI-driven ATP synthesis was found in $143B^{-/-}$ and $HCT116^{-/-}$ cells compared to controls, while CII- and CIII-mediated ATP synthesis were not significantly affected (26). We here show that such residual CI-driven ATP production is completely abolished in $143B^{-/-}$ cells by the treatment with 50 µg/mL CAP (Fig. 1F). Further, the presence of a residual fully assembled and functional CI was also evident in the mouse B16-F10 melanoma cell model lacking Ndufs3 ($B16^{-/-}$), ruling out the possibility of a human-specific compensatory mechanism (Supplementary Fig. 3A-C).

To better understand the dynamics of CI assembly upon ablation of NDUFS3, we investigated 143B cells in which the expression of NDUFS3 can be fully repressed by doxycycline (Dox) in a Tet-Off system, hereafter referred as $143B^{-/-NDUFS3}$ (Kurelac et al., 2019). Treatment with 100 ng/mL Dox induced a progressive reduction of NDUFS3 that started promptly after 12h until the subunit was undetectable after 4 or 8 days of incubation (Fig. 2A and Supplementary Fig. 3D). These doses and treatment times did not affect mitochondrial translation, as shown by the levels of mtDNA-encoded subunit MT-CO2 (Supplementary Fig. 3E). CI-IGA was still detectable in both isolated CI and in SCs at the same time points in which the presence of NDUFS3 was undetectable (Fig. 2B and Supplementary Fig. 3F). The gradual decrease of NDUFS3 levels was not always followed by the reduction in the steady-state levels of other CI subunits, as in the case of NDUFB8, NDUFB6 and NDUFA9, which remained consistently stable after NDUFS3 repression (Fig. 2C). Conversely, the reduction of NDUFS3 was followed by a progressive decrease of fully assembled CI and accumulation of subcomplexes containing NDUFB8 and NDUFB6, while CIII and CIV were not affected (Fig. 2D-E). These data are in agreement with the presence of subcomplexes with positive immunodetection for NDUFB8 and NDUFB6 found in $143B^{-/-}$ and $HCT116^{-/-}$ cells and may explain the high levels of these subunits after NDUFS3 repression. However, a residual CI was found in SCs after 8 days of Dox treatment of $143B^{-/-NDUFS3}$, as highlighted by positive staining for all the tested CI, CIII and CIV subunits (Fig. 2D-E). Moreover, fully assembled CI containing NDUFB8

was evident also in its isolated form after 8 days of incubation of 143B$^{-/-NDUFS3}$ with 100 ng/mL Dox (Supplementary Fig. 3G). On the other hand, the incubation for 8 days with 100 ng/mL Dox together with 50µg/mL CAP inhibited mitochondrial translation and thus mtDNA-encoded CI subunits resulting in the complete absence of the enzyme (Fig. 2B and Supplementary Fig. 3E).

Overall, these data demonstrate that despite the absence of NDUFS3 a residual but clearly detectable amount of active CI associated into SCs is present in both human and mouse cell models, without affecting the composition and function of the remaining OXPHOS system, whereas mtDNA-encoded subunits are an absolute requirement. The possibility that the detected CI is just residual enzyme that has not completely disassembled can be ruled out, as the same treatment times with inhibitors of mitochondrial translation produce the complete disappearance of the complex (8). Cell models with constitutive ablation of *NDUFS3* might have adapted to the persistent absence of the subunit during the process of clonal selection and expansion, developing, for instance, an alternative CI assembly pathway to overcome the lack of this core subunit. However, the Tet-Off model provides a system in which the activation of such adaptive program is highly unlikely, supporting the idea of an alternative assembly route, not involving NDUFS3 that enables the building of a small proportion of functional CI.

Progressive loss of NDUFS3 reveals the modular dynamics of CI disassembly

The Tet-Off 143B$^{-/-NDUFS3}$ model provided a dynamic system in which the kinetic of CI disassembly could be followed upon the progressive depletion of NDUFS3. Changes in mitochondrial protein levels relative to the untreated 143B$^{-/-NDUFS3}$ cells were analyzed upon treatment with 100 ng/mL Dox after 2, 4 and 8 days by quantitative proteomics using SILAC and validated via western blotting and immunodetection (Fig. 3A and Supplementary Fig. 4A). When the fold change values for each protein in the two reciprocal experiments were plotted (log2 H/L ratios of one experiment in the x axis; -log2 H/L rations of the second experiment in the y axis), the protein points distributed over a 45º diagonal line, reflecting the correlation between the two duplicate experiments (Fig. 3A). Most of the detected proteins were unaffected by the progressive reduction of NDUFS3 levels, as

they clustered around the axis origin. In particular, subunits of CIII and CIV were found not altered upon treatment with 100 ng/mL Dox up to 8 days (Fig. 3A), confirming the stability of these complexes when NDUFS3 is repressed. On the other hand, significant progressive changes in the relative abundance of CI subunits and assembly factors were detected (Fig. 3A-B and Supplementary Fig. 4B). The coverage of CI subunits was very high ranging from 77% to 82% of CI subunits detected in the time-course experiments. In agreement with western blotting data, NDUFS3 steady state levels underwent a progressive severe decrease upon treatment with Dox that reached a logarithmic fold change of -3.73±0.27 (approximately 13-fold decrease) after 8 days (Fig. 3A-B). Q-module subunits (NDUFS2, NDUFS7, NDUFS8 and NDUFA5) were the first to be downregulated after NDUFS3 depletion, being significantly reduced already after 2 days of Dox treatment (Fig. 3A-C). The levels of N-module subunits (NDUFV1, NDUFV2, NDUFV3-L, NDUFS1, NDUFS4, NDUFS6, NDUFA2, NDUFA12, NDUFA6 and NDUFA12) were less affected after 2 days of NDUFS3 suppression, reaching a significant reduction after 4 and 8 days (Fig. 3A-C). Interestingly, subunits NDUFA6 and NDUFA7, whose module assignment is still debated, clustered with N-module subunits with a reduction of -2.31 ± 0.06 and -2.22 ± 0.01 respectively, suggesting that they may belong to this module. The stability of the P-module subunits resulted less homogeneous, as some of them are not affected by NDUFS3 repression (Fig. 3A-C). In particular, ND1-module subunits (ND1, NDUFA3, NDUFA8 and NDUFA13) were markedly destabilized by NDUFS3 suppression and clustered together with Q- and N-modules after 8 days of Dox treatment. Among ND1-module subunits, NDUFA3 was the most stable with a $\log_2$ ratio of -1.89±0.35. At the earliest time-point ND2-, ND4- and ND5-modules were mainly unaffected by NDUFS3 repression. However, subunits belonging to ND2-module (ND2, ND3, NDUFA10, NDUFS5 and NDUFC2) became more unstable after 8 days of Dox treatment. Interestingly, NDUFA10 and NDUFS5 protein levels clustered with ND1-module subunits rather than those belonging to the ND2-module, with a logarithmic fold change of -2.86±0.17 and -2.92±0.15 respectively. On the other hand, the ND4- and ND5-modules are particularly stable upon NDUFS3

depletion, with their levels unchanged at all times with respect to those of the control. The permanence of the distal membrane arm subunits was most probably due to the formation of stable CI subassemblies, as shown by the accumulation of a NDUFB6- and NDUFB8-containing subassembly intermediate (Fig. 1E, Fig. 2D-E and Supplementary Fig. 1G). NDUFA9, NDUFA11, NDUFB4 and NDUFB6 subunits are shown as a group termed "uncertain" as their module assignment is still unclear (12).

Most CI assembly factors resulted unchanged upon NDUFS3 repression (Supplementary Fig. 4A-B), with the exception of NDUFAF3, NDUFAF4, FOXRED1 and ATP5SL. Interestingly, the Q-module assembly factors NDUFAF3 and NDUFAF4 levels declined significantly already after 2-days of NDUFS3 repression and remained very low during the whole time-course. Although to a lesser extent, the levels of two assembly factors of the ND4-module FOXRED1 and ATP5SL (6, 8, 28, 29) were also significantly reduced in NDUFS3-repressed cells, in contrast with those of the structural subunits of the same module, which were consistently unchanged. Therefore, these assembly factors may belong to another module(s) or have a role in the joining of the ND4-module with the others. These data depict a dynamic scenario for CI disassembly also as a modular process in which the Q-module is promptly affected by the reduced availability of NDUFS3, followed by the nearby N-module and proximal P-module, while levels of the subunits belonging to the distal ND4- and ND5-modules are not affected and accumulate in stable assembly intermediates most likely containing NDUFB6 and NDUFB8.

TMEM126A is a novel assembly factor of respiratory CI

The accumulation of such assembly intermediates prompted the search for proteins that would be upregulated upon NDUFS3 repression and likely to interact with the accumulated ND4- and ND5-modules. Proteins with these characteristics are *bona fide* candidates to be CI assembly factors. To this end, immunopurification of CI using SILAC samples of $143B^{-/-NDUFS3}$ cells harvested after 2, 4 and 8 days of NDUFS3 repression was performed (Supplementary Fig. 5A). The coverage of these experiments was optimal ranging from 40 to 43 out of 44 different CI detected subunits. Among all

the proteins preferentially enriched upon NDUFS3 repression, TMEM126A/Opa7 was the only one showing significantly increased amounts after 4 and 8 days of Dox treatment (Supplementary Fig. 5A). The accumulation of TMEM126A in immunopurified fractions was not mirrored in a general increase of the protein in total lysates and mitochondrial fractions from Tet-Off model upon progressive repression of NDUFS3 (Fig. 3A and Fig. 4A). Indeed, TMEM126A resulted specifically accumulated in the CI subassembly containing NDUFB6 corresponding to the stable ND4-module found in proteomics (Fig. 4B6). The uncharacterized mitochondrial protein TMEM126A is a paralog of the CI assembly factor TMEM126B (30) and mutations in *TMEM126A* (OMIM, #612988) have been found in multiple families affected by non-syndromic autosomal recessive optic atrophy (arOA) (OMIM, #612989). However, its function and putative role in mitochondrial respiratory chain biogenesis has never been depicted, representing a very promising CI assembly factor candidate and relevant for disease. To demonstrate this hypothesis, we investigated CI assembly and function in commercially available HAP1 cells in which *TMEM126A* was knocked out by CRISPR/Cas9 ($HAP1^{-/-}$, Horizon Discovery, #HZGHC05796c002). In these cells, the lack of TMEM126A was associated with a reduction of the steady state levels of several subunits of CI, while those belonging to CIII and CIV were not affected (Fig. 4C-D). From a functional point of view, rotenone-sensitive CI activity was strongly reduced in $HAP1^{-/-}$ compared to controls (Fig. 4E and Supplementary Fig. 5B), whereas CIII and CIV activities were not affected (Supplementary Fig. 5C), indicating that loss of TMEM126A induced an isolated CI deficiency. Such a functional defect of CI was also translated into a reduced respiratory capacity in the $HAP1^{-/-}$ cells (Fig. 4F). In accordance, $HAP1^{-/-}$ were not able to survive under metabolic stress conditions, i.e. 5 mM galactose as carbon source, and the same cells showed reduced proliferation when grown in medium containing 25 mM glucose (Fig. 4G and Supplementary Fig. 5D-E). Overall, these data demonstrate that TMEM126A is responsible for the maintenance of a functional OXPHOS system, most probably acting as an assembly factor necessary for the correct biogenesis of CI by interacting

with the ND4-module and allowing this module to join the rest of modules to complete the assembly.

Discussion

In this study, we have investigated the role of the core subunit NDUFS3 in the assembly, stability and function of respiratory CI. By exploiting multiple unique cell models in which we have selectively knocked out or repressed NDUFS3, we demonstrate that a small portion of fully assembled and functional respiratory CI is present at the level of SCs when NDUFS3 is absent. NDUFS3 is a core subunit, extremely conserved across evolution and believed to be essential for CI assembly, being an early-entry subunit of the Q-module (9, 12, 19). However, although the lack of NDUFS3 strongly affects the amount of fully assembled and functional CI, a residual activity was evident in our models derived from three different human and murine cancer cell lines. It is important to note that the existence of residual CI is evident also in differentiated mouse skeletal muscle tissue of a conditional *Ndufs3* KO model (25), indicating that such phenotype is not a prerogative of cancer cells. In particular, the presence of the N-module subunits at the levels of SCs indicated completion of active CI assembly. Our hypothesis is that an alternative, although unfavorable, route for CI assembly can be followed when NDUFS3 is missing and that the presence of SCs may help to stabilize CI missing NDUFS3 activating its function. In this frame, SCs seem to provide a platform for the stabilization of mature CI as suggested by others (17, 18). Whether this alternative route can be followed also when other CI subunits are missing or is exclusive of NDUFS3 remains to be elucidated. Indeed, NDUFS3 has the peculiarity of being a core subunit without real catalytic activity and when it is missing, several other subunits are reduced but not completely absent, supporting the assembly of functional CI. Regarding, mtDNA-encoded subunits we here show that they are pivotal for the assembly of the enzyme, as no residual CI is detected in presence of a truncative mutation of *MT-ND1* or when mtDNA is depleted (Rho0 cells), but it also disappears when mitochondrial translation is inhibited by CAP. On the other hand, the ablation of

accessory subunits was shown to impact on CI assembly to a different extent depending on the role and topology of the subunit (6).

The NDUFS3 Tet-Off system provided an extremely valuable tool for the analysis of CI disassembly and for the assignment of yet uncertain subunits to specific modules. Upon NDUFS3 repression, a whole CI remains stable for about two days and then start to decrease, indicating that the complex turnover takes place within this timeframe (20). The kinetics of the reduction of CI subunit amounts reported here is in agreement with the current CI organization and modular assembly models (6, 8). Q-module subunits were significantly reduced merely after 2 days of NDUFS3 repression, followed by N-module subunits, confirming that the assembly of the N-module is independent from the Q-module, but also that their interaction is necessary to build the whole CI. Regarding the membrane arm modules, the most affected subunits are those belonging to the proximal P-module (ND1 and ND2 submodules), while the distal P-module's subunits (ND4- and ND5-modules) remain stable and form a subcomplex of about 350 kDa containing NDUFB6 and NDUFB8 which progressively accumulates with the disassembly of the fully assembled enzyme. The pattern of steady state levels of individual subunits may help the process of module assignment for some subunits whose localization is still uncertain. For example, our data support the assignment of NDUFA6 and NDUFA7 to the N-module as proposed by Stroud et al. and in contrast with the most recent model (6, 8). Similarly, NDUFB6 clustered with ND4-module subunits and remains consistently stable across the different time points, thus suggesting its assignment to this module. Interestingly, ND2-module subunits NDUFA10 and NDUFS5 behaved differently relative to the other module subunits being markedly affected by NDUFS3 repression. This discrepancy was observed across the time-points and their fold changes were analogue to those of N-module subunits. Since NDUFA10 and NDUFS5 form extensive interactions with Q- and ND1-modules, one possibility is that the assembly impairment of such modules could be transferred to these subunits in the case in which they are added to a preformed ND2-module.

Interestingly, the lack of NDUFS3 and the consequent reduction of CI do not affect the stability of other MRC complexes, in particular $CIII_2$ and CIV, resulting in an isolated CI impairment. This is a common phenomenon in the cases where the origin of the mitochondrial defect are mutations in structural or ancillary CI proteins, where the biochemical manifestation is always isolated CI deficiency (31). This is different from mutations causing a strong impairment in $CIII_2$ biogenesis where there is a secondary loss of CI and, occasionally, CIV activity (32–37). In some cases, strong defects in CIV biogenesis also have an impact on CI assembly or stability (38). In human cells, the near totality (90-95%) of CI appears associated with SCs when the mitochondria are solubilized with a mild detergent such as digitonin, whereas approximately 50% of $CIII_2$ is inside SCs and 90% or CIV is in the 'free' monomeric form (15). There is growing evidence in the literature showing alternative maturation routes for $CIII_2$ and CIV depending on whether they are in the free or in the SC-associated forms (39–41). Moreover, only a residual amount of CI is able to mature when $CIII_2$ is absent (18), therefore, the efficient incorporation of the N-module of CI only occurs in the context of the SCs, at least in human cells (18, 40). The dependent assembly of CI on one hand, and independent biogenesis of $CIII_2$ and CIV on the other, would explain why defects in the latter induce secondary defects in CI assembly but not the opposite. However, this phenomenon was also viewed as the consequence of an oxidative damage-triggered degradation, by yet undescribed mechanisms, of fully assembled CI if not associated with $CIII_2$ (32, 42).

Finally yet importantly, we found that the mitochondrial protein TMEM126A/Opa7 is consistently accumulated with distal P-module subcomplexes upon NDUFS3 repression. *TMEM126A* encodes an evolutionary conserved transmembrane mitochondrial protein of yet unknown function. TMEM126A shows a high sequence homology with the assembly factor TMEM126B, which is part of the mitochondrial complex I intermediate assembly (MCIA) complex which is necessary for the assembly of the ND2-module (43, 44). The homozygous nonsense c.163C>T founder mutation (p.Arg55X) in *TMEM126A* has been shown to be pathogenic in both syndromic and non-syndromic forms of autosomal recessive optic atrophy (arOA) (45–48). A partial CI deficiency and elevated

lactic acid levels in blood, a typical sign of OXPHOS dysfunction, have been reported in some patients (46, 47). Moreover, downregulation of TMEM126A is associated with poor prognosis in breast cancer and increases metastatic properties of breast cancer cells through the activation of epithelial-to-mesenchymal transition (EMT) (49). Despite the considerable involvement in human pathology, TMEM126A function remained unexplored. We here demonstrate that this protein is a factor necessary for correct biogenesis and function of the mitochondrial respiratory chain, in particular of CI, through the stabilization of the submodule containing MT-ND4 within the distal P-module. Two main lines of evidence support the fact that TMEM126A is involved in this specific aspect within the CI assembly pathway. First, there is an accumulation of subunits belonging to this module inside stable subassembly species in the cells lacking NDUFS3, while other topological distinct subunits are strongly reduced. Our proteomic and interaction analysis demonstrated that TMEM126A is also accumulated in these cells and physically interacts with the remaining CI subunits. Secondly, cells lacking TMEM126A are deficient in CI function and biogenesis.

Conclusions

We here consistently show that, although at low levels and very surprisingly, fully assembled and functional CI can exist also in absence of the core subunit NDUFS3. This suggests the existence of a less efficient biogenetical pathway that spares NDUFS3 that may guarantee a minimal CI activity in these conditions. This residual CI is fully functional and able to interact with complexes III and IV forming respiratory supercomplexes (SCs), the formation of which promotes CI assembly and in this frame they may acting as stabilizing factors of such residual CI. We also show that the disassembly of CI induced by progressive depletion of NDUFS3 is a modular process and revealed interactions between subunits that had not been described before. Lastly, we identify TMEM126A/Opa7 as a biogenetic factor of respiratory CI, most probably acting on the assembly of the distal P-module.

Material and methods

Cell lines

Human osteosarcoma 143B TK^- and colorectal cancer HCT116 cell lines bearing the homozygous c.9_10insCGGCG frameshift mutation in *NDUFS3*, which resulted in a premature stop codon and the truncation of the protein (p.Val6Alafs*3), were analyzed relative to their isogenic control ($143B^{+/+}$ and $HCT116^{+/+}$). These NDUFS3 knockout cells, referred as $143B^{-/-}$ and $HCT116^{-/-}$, were generated as previously reported (26). 143B Tk^- cybrid cells carrying the truncative frameshift m.3571insC/*MT-ND1* mutation were used as well. Specifically, the previously characterized homoplasmic cells (OS) and heteroplasmic cells with 93% of mutated *MT-ND1* (OS-93) were used (50, 51, 27). 143B Tk^- mtDNA-depleted cells (ρ0) provided CI-negative control. Doxycycline-inducible NDUFS3 knockout 143B cells (referred as $143B^{-/-\ NDUFS3}$) were also used. They were generated re-expressing *NDUFS3* using the Tet-Off inducible system ensuring the transcriptional repression of the complemented gene in the presence of doxycycline as previously described (26).

B16-F10 murine melanoma cell lines were purchased from ATCC (#CRL-6475). Cells were cultivated in Dulbecco's modified Eagle medium (DMEM) High Glucose (Euroclone #ECM0749L), supplemented with 10% FBS (Euroclone #ECS0180L), L-glutamine (2 mM, Euroclone #ECB3000D), penicillin/streptomycin (1x, Euroclone #ECB3001D) and uridine (50 µg/mL, Sigma-Aldrich #U3003) in an incubator with a humidified atmosphere at 5% CO2 and 37°C.

Human chronic myeloid leukemia HAP1 cell line with a 79 bp-insertion in *TMEM126A* exon 4 ($HAP1^{-/-}$; Horizon Discovery, #HZGHC05796c002) and their relative wild-type control ($HAP1^{+/+}$) were used to demonstrate the role of TMEM126A.

Genome editing

CRISPR/Cas9 system was used to introduce a frameshift mutation in *Ndufs3* gene in B16-F10 murine melanoma cell lines. In detail, Cas9 protein (Invitrogen #A36497) was transfected by following manufacturer's instructions using Lipofectamine™ CRISPRMAX™ Cas9 Transfection Reagent (Invitrogen #CMAX00015) together with synthetic RNA guides designed by Deskgen and

purchased from Synthego. Exon 1 targeting guide ACATGGCGGCGGCTGCAGCC with PAM sequence AGG was used to create clone E6(1) and Exon 3 targeting guide TTGTGGGTCACATCACTCCG with PAM sequence GGG was used to create G4(2). Cells were split 48 hours after transfection and DNA was extracted using Mammalian Genomic DNA Miniprep Kit (Sigma-Aldrich #G1N350). Non-homologous repair efficiency was evaluated by Sanger Sequencing using KAPA2G Taq polymerase (Kapa Biosystems #KK5601) and Big Dye protocol (Life Technologies #4337451). In particular, for Exon 1 58°C annealing temperature was used for the PCR reaction, with primers forward TGCGTCTTCTTCTCTTCGGC and reverse CAACGAAAGGCCCCAGCTAA. For Exon 3 61°C annealing temperature was used for the PCR reaction, with primers forward CTGTAACTCCAGTCTCAGGGA and reverse CACACTGCAGGGATCACTTG. Manual clonal selection was performed in order to identify the cells with frameshift *Ndufs3* mutations, leading to the generation of a pool of clones carrying the homozygous c.328A>G and c.330_331InsCT mutations. DNA extraction from 96-well plates was performed using 8 µl of Lysis Solution (Sigma-Aldrich #L3289) and 80 µl of Neutralization Buffer (Sigma-Aldrich #N9784) per sample, following manufacturer's instructions.

Cell maintenance and treatments

143B, HCT116 and B16-F10 cell lines were grown in high-glucose Dulbecco's Modified Eagle's Medium (DMEM) plus Glutamax and sodium pyruvate (Gibco-Thermo Fisher Scientific, #31966) supplemented with 10% fetal bovine serum (Gibco-Thermo Fisher Scientific, #10270), and 50 µg/mL uridine (Sigma-Aldrich, #U3003), in an incubator with an humidified atmosphere at 5% CO_2 and 37°C. $143B^{-/-NDUFS3}$ cells were grown in the same medium but with addition of 100 µg/mL G418 (Sigma-Aldrich, # A1720) and 50 µg/mL puromycin (Thermo Fisher Scientific, #A1113803) to sustain the selective pressure. In this cell model, expression of NDUFS3 was repressed by addition of 100 ng/mL doxycycline (Sigma-Aldrich, #D9891). For the inhibition of mitochondrial translation 50 µg/mL chloramphenicol (Fisiopharm, #J01BA01) was used. HAP1 cell lines were cultured in Iscove's Modified Dulbecco's Medium (IMDM) with 10% FBS, 1% Pen/Strep, and 50

μg/mL uridine. For SILAC experiments, 143B$^{-/-NDUFS3}$ cells were grown in SILAC DMEM (Gibco Thermo Fisher Scientific, #88364) added with either isotopically labelled 152.1 mg/L L-Lysine-$^{15}N_2{}^{13}C_6$ (Sigma-Aldrich, #608041) plus 87.8 mg/L L-Arginine-$^{15}N_4{}^{13}C_6$ (Sigma-Aldrich, #608041) ("Heavy" medium), or unlabelled 143.8 mg/L L-Lysine (Sigma-Aldrich, #L8662) and 69.3 mg/L L-Arginine (Sigma-Aldrich, #A8094) ("Light" medium). Both differentially labelled media were supplemented also with 10% dialyzed serum (Invitrogen, #26400-044), 50 μg/mL uridine, 100 μg/mL G418, 50 μg/mL puromycin and 200 mg/mL L-Proline (Sigma-Aldrich, #P5607). Incorporation of the "Heavy" amino acids into the cells proteins was completed after approximately 9 passages (52). Cell lines were regularly tested for mycoplasma.

SDS-PAGE

Whole-cell lysates were obtained incubating cell pellets with a Lysis Buffer (2% *n*-dodecyl β-d-maltoside (DDM) (Thermo Scientific, #89903) plus 1X protease inhibitor cocktail (Roche, # 11697498001) in PBS) for 20 min at 4°C. Protein concentration in the extracts was measured with a Nanodrop UV-visible spectrophotometer at λ= 280nm. 25 μg of total protein were combined with 2X Laemmli Sample Buffer (2% sodium dodecyl sulphate (SDS), 4.6% β-mercaptoethanol, 20% glycerol, 0.025% bromophenol blue and 62.5 mM Tris/HCl at pH 6.8) in one-to-one ratio, loaded on pre-cast NuPAGE™ 4-12% or 12% Bis-Tris gels (Invitrogen, #NP0321, #NP0322, #NP0341, #NP0342) and resolved in a electrophoresis cell at 100 V for approximately 2 hours at RT. Either NuPAGE™ MOPS or MES SDS Running Buffers were used (Invitrogen, #NP0001, #NP0002*)*. Precision Plus Protein™ Standard (Bio-Rad, #1610374) was used for molecular weight (MW) estimation.

Blue-Native PAGE

For the preparation of samples for Blue-Native PAGE, firstly mitochondrial-enriched fractions were obtained by digitonin treatment (53). Briefly, cells were harvested by trypsinization, 5-8x10^6 cell pellets were washed twice and resuspended in cold DPBS and incubated 10 min on ice with 2 mg/mL digitonin (Calbiochem, #3000410-5GM). Next, cold DPBS was added and a centrifugation

at 10,000 g for 10 min and 4°C was performed. The obtained mitochondrial-enriched fractions were solubilized in a Solubilization Buffer (1.5 M aminocaproic acid, 50 mM Bis-Tris/HCl at pH 7). Proteins were quantified by a detergent-compatible Lowry-based method (Bio-Rad DC Protein Assay), solubilized either with 1.6 µg DDM/µg total proteins or 4 µg digitonin/µg total proteins and incubated at 4°C for 5 min (54).Insoluble material was removed by a centrifugation (18,000 g at 4°C for 30 min) and Sample Buffer (750 mM aminocaproic acid, 50 mM Bis-Tris/HCl pH 7, 0.5 mM EDTA and 5% Coomassie Blue G250) was added. For 1D-BN PAGE, 50-75 µg of proteins were loaded on Pre-cast Native PAGE 3-12% Bis-Tris gels (Invitrogen, #BN2011BX10) at 150 V and 4°C for 4 hours. Cathode Buffer A containing 1x NativePAGE™ Running Buffer (Invitrogen, #BN2001) plus 1x NativePAGE™ Cathode Buffer Additive (Invitrogen, #BN2002); Cathode Buffer B containing 1x NativePAGE™ Running Buffer and 0.1x NativePAGE™ Cathode Buffer Additive; and Anode Buffer consisting of 1x NativePAGE™ Running Buffer were used.

2D BN-PAGE

1D BN-PAGE lanes were excised from the gel and incubated with a Denaturing Solution (1% 2-mercaptoethanol, 1% SDS) at RT for 1 hour. Then, the lanes were inserted in denaturing Pre-cast NuPAGE™ 4-12% Bis-Tris Gels (Invitrogen, #NP0326) in a 90° orientation and separated in either MES or MOPS SDS Running Buffer at 100 V for approximately 2 hours at RT.

Western blotting and immunodetection

Proteins resolved by either SDS-PAGE or 2D BN-PAGE were transferred onto a polyvinylidene difluoride (PVDF) membrane. The blotting was performed at 100 V for 1 hour at 4 °C in Tris-Glycine Transfer Buffer (12.5 mM Tris, 96 mM glycine, 20% Methanol, 0.025% SDS). Membranes were blocked 1 hour at RT with 5% powdered skimmed milk in PBS containing 0,1 % tween 20 (PBS-T), washed three times for 10 min in PBS-T and incubated o.n. at 4°C with the following primary antibodies diluted in a blocking solution containing 3% BSA in PBS-T: anti-TMEM126A (Atlas,#HPA046648); anti-CS (Abcam, #ab96600) 1:1000; anti-VDAC (Abcam, #ab154856) 1:1000; anti-MTCO1 (Abcam, #ab14705) 1:1000; anti-MT-CO2 (Abcam, #ab110258) 1:1000; anti-

UQCRC2 (Abcam, #ab14745) 1:1000; anti-CYC1 (Proteintech, #10242-1-AP) 1:1000; anti-UQCRFS1 (Abcam, #ab14746) 1:1000; anti-NDUFA9 (Abcam, #ab14713) 1:1000; anti-NDUFS3 (Abcam, #ab110246) 1:1000 or 1:500; anti-NDUFS8 (Santa Cruz Biotechnology, #SC-515527) 1:1000; anti-NDUFB8 (Abcam, #ab110242) 1:1000; anti-NDUFB11 (Proteintech, #16720-1-AP) 1:700; anti-NDUFA12 (Sigma-Aldrich, #SAB2701046) 1:1000; anti-NDUFB6 (Abcam, #ab110244) 1:1000; anti-NDUFS6 (Abcam, #ab195807) 1:1000; anti-SDHB (Abcam, #ab147114) 1:1000; anti-SDHA (Abcam, #ab14715) 1:1000; anti-Hsp70 (Abcam, #ab2787) 1:1000; anti-β-actin (Sigma-Aldrich, #AI978) 1:1000; anti-β-tubulin (Sigma-Aldrich, #T5201) 1:1000; anti-TIMMDC1 (homemade, a generous gift from Prof. John E. Walker's group) 1:2500. Then, three washes of 10 min in PBS-T were performed and membranes were incubated 1 hour at RT with the following 1:5000 or 1:2500 horseradish peroxidase conjugated secondary antibodies in 1% milk in PBS-T: anti-mouse (Promega, #W402B), anti-rabbit (Promega, #W401B) and anti-chicken (Promega, #G1351). Proteins resolved by 1D BN-PAGE were electroblotted as above, except that the blotting was performed at 300 mA for 1 hour at 4°C in Bicarbonate Transfer Buffer (10 mM $NaHCO_3$ and 3 mM Na_2CO_3). To visualize the immunoreactive bands, ECL Western Blotting Reagents (GE Healthcare, #RPN2106) were used. When performed, band signal intensities were quantified by densitometry using ImageJ and 2-way ANOVA with Sidak's post-hoc test was used for multiple comparison statistical analysis.

Enzymatic activity assays

Crude mitochondria were used to assess respiratory chain enzymatic activities. A pellet of 15-20 x 10^6 cells was suspended in ice-cold Sucrose-Mannitol Buffer (200 mM mannitol, 70 mM sucrose, 1 mM EGTA and 10 mM Tris-HCl at pH 7.6) and homogenized using a glass/teflon Potter homogenizer. The obtained sample was centrifuged at 600 g for 10 min at 4 °C to discard unbroken cells and nuclei. The resulting supernatant was centrifuged at 10,000 g for 20 min at 4 °C to separate crude mitochondria from the remaining sub-cellular fractions of the sample. CI (NADH:DB:DCIP oxidoreductase), CI+CIII (NADH:cytochrome *c* reductase), CII

(succinate/DCPIP), CIII activity (cytochrome *c*/DBH2), and CIV (cytochrome *c* oxidase) activities were measured as previously described (55). Each specific activity was normalized to protein content and citrate synthase (DTNB:oxaloacetate) activity. CI-IGA assays were performed either on 1D BN-PAGE or High-Resolution Clear Native PAGE (hrCNE) gels. The latter was electrophoresed as described (27) and incubated with 2 mM Tris-Cl (pH 7.4), 0.15 mM NADH, and 2.5 mg/mL 3-(4,5-dimethylthiazol-2-yl)-2,5-diphenyltetrazolium bromide (MTT) o.n. at RT. 1D BN-PAGE gels were incubated with solution containing 0.5 M Tris/HCl (pH 7.4), 0.1 mg/mL NADH, 1mg/mL nitro tetrazolium blue (NTB) at RT o.n.

ATP synthesis rate assay

The rate of mitochondrial ATP synthesis driven by CI, CII, and CIII was measured in digitonin-permeabilized cells treated or not with 50 µg/mL chloramphenicol as previously detailed (55). Briefly, cells (10×10^6 /mL) were suspended in a buffer containing 150 mM KCl, 25 mM Tris–HCl, 2 mM EDTA (ethylenediaminetetraacetic acid), 0.1% bovine serum albumin, 10 mM potassium phosphate, 0.1 mM $MgCl_2$, pH 7.4, and incubated with 50 µg/mL digitonin until 90–100% of cells were positive to Trypan Blue staining. Aliquots of 3×10^5 permeabilized cells were incubated in the same buffer in the presence of the adenylyl kinase inhibitor P_1,P_5-di(adenosine-5′) pentaphosphate (0.1 mM) and OXPHOS complexes substrates, chemiluminescence was determined as a function of time with Sirius L Tube luminometer (Titertek-Berthold, Pforzheim, Germany). The chemiluminescence signal was calibrated with 11 µM internal ATP standard after the addition of 1 µM oligomycin. 1 µM rotenone was added instead of oligomycin to determine the specific CI-driven ATP synthesis. The rates of the ATP synthesis were normalized to protein content and citrate synthase (CS) activity.

Quantitative Proteomics

Proteomic analyses were performed on mitochondrial enriched fractions and SILAC relative quantification approach was used as previously described (56). In the present study, aliquots from each sample were retained before performing CI immunoprecipitation and directly analyzed by

mass spectrometry (MS). For CI co-immunopurification, mitochondrial-enriched fractions were incubated o.n. at 4°C with Complex I Immunocapture Kit (Abcam; #ab109711) suspension. Tryptic peptide mixtures were resolved by Nanoscale High Performance Liquid Chromatography (nano-HPLC) in a C18 reverse phase column (75 µm x 100 mm) with a gradient of acetonitrile in 0.1% formic acid and a flow rate of 300 nL/min. The eluate was analyzed by Q Exactive™ Plus Hybrid Quadrupole-Orbitrap™ Mass Spectrometer (Thermo Fisher Scientific) operating in mass tandem (MS/MS) mode. Protein identification and quantification were performed with MaxQuant computational platform (57, 58). For the relative quantification, MaxQuant calculated the ratios between the peak intensities of heavy- and light-labelled peptide pairs (H/L ratio). Each proteomic analysis was performed in duplicate: in one duplicate experiment, the heavy-labelled Dox-treated cells were mixed, in a one-to-one ratio, with the light-labelled untreated ones; in the other the labelling was inverted. Fold changes for each protein were plotted in scatter plots with the $\log_2$H/L ratios of one experiment in the x axis and -$\log_2$H/L ratios of the second experiment in the y axis. Correlation between the two duplicate experiments was reflected by the distribution of the protein over a 45º diagonal line of the scatter plots. Statistical significances of the differences for enriched and depleted proteins in each reciprocal experiment were determined by applying the B-significance test with Perseus (59, 60).

Cell viability assay

HAP1 cell viability was evaluated by sulforhodamine B (SRB) assay. 30,000 cells/well were seeded in 24-well plates and incubated o.n.. Then, IMDM was replaced with either glucose-free and galactose-containing (5 mM) DMEM or glucose-containing (25 mM) DMEM. After 24, 48 and 72 hours of incubation, medium was replaced with a fresh one, 10% trichloroacetic acid (TCA) was added, and the plates were incubated for 1 hour at 4°C to fix the cells. 5 washes in water were performed. When the plates were dry, proteins of the fixed cells were stained by an incubation with 0.4% SRB for 30 minutes at RT. SRB was removed and 5 washes with 1% acetic acid were carried out to eliminate the residual SRB. Finally, the SRB bound to the proteins was solubilized in 10 mM

Tris and the absorbance at 560 nm was read in a Victor2 plate reader (Perkin-Elmer). Measurements were blank corrected.

Oxygen consumption rate

Mitochondrial respiration was evaluated using the Seahorse XFe Cell Mito Stress Test Kit (Agilent #103015-100) following the manufacturer instructions. Cells were seeded (40×10^4 cells/well) in 80 µL of IMDM medium into XFe96 cell culture plate and allowed to attach for 24 h. Cell culture media was replaced with Seahorse XF DMEM Medium, pH 7.4 (Agilent #103575-100). OCR was measured over a 3 min period, followed by 3 min of mixing and re-oxygenation of the medium. For Mito Stress Test, complete growth medium was replaced with 180 µL of unbuffered XF medium supplemented with 10 mM glucose pH 7.4 pre-warmed at 37 °C. Cells were incubated at 37 °C for 30 min to allow temperature and pH equilibration. After 6 OCR baseline measurements, 1 µM oligomycin, 0.25 µM carbonyl cyanide-p-trifluoromethoxyphenylhydrazone (FCCP), and 0.5 µM rotenone plus 0.5 µM antimycin A were sequentially added to each. Three measurements of OCR were obtained following injection of each drug and drug concentrations optimized on cell lines prior to experiments. At the end of each experiment, the medium was removed and SRB assay was performed to determine the amount of total cell proteins as described above. OCR data were normalized to total protein levels (SRB protein assay) in each well. Each cell line was represented at least four wells per experiment ($n = 4$ replicate experiments). Data are normalized on SRB absorbance and expressed as pmoles of O_2 per minute.

Statistics

GraphPad Prism v.7 (GraphPad Software Inc., San Diego, CA, USA) was used to perform statistical tests and create bar plots and graphs. Unless stated otherwise, a two-tailed unpaired Student's t-tests assuming equal variance were performed to compare averages. For each experiment, at least three biological replicates were analyzed.

Acknowledgments

This work was supported by University of Bologna AlmaIdea Junior grant INTACT to LI, by EU H2020 ITN Marie Curie project TRANSMIT [grant number GA722605] to AMP, by Italian Ministry of Health grant DISCO TRIP [grant number GR-2013-02356666] to GG and by Core Grant from the Medical Research Council (Grant MC_UU_00015/5) to MZ. MDL was supported by Associazione Italiana Ricerca sul Cancro (AIRC) fellowship. We thank Fondazione Dal Monte (Bologna, Italy) and Centro Studi della Barbariga (Padua, Italy) for the economic support finalized to the acquisition of instruments Seahorse XFe96 and Jasco V550 spectrophotometer, respectively.

We thank Dr. Joe Carroll and Prof. John E. Walker (Mitochondrial Biology Unit, Cambridge) for the insightful discussion on the role of TMEM126A; Ana Maria Rusu and Prof. F. Musiani (University of Bologna) for the technical suggestion in the production of Complex I structure pictures.

Author contributions

Conceptualization, M.Z., A.M.P., E.F.V. and L.I.; Methodology, M.D.L., I.K., N.U.G., S.D., I.F., E.F.V. and L.I; Investigation, L.D.A., E.A., M.D.L., S.D. and L.I.; Formal analysis, L.D.A., E.A., S.D. and L.I.; Writing – Original Draft, L.D.A., E.A., G.G., A.M.P., E.F.V. and L.I.; Review & Editing, all the authors; Funding Acquisition, M.Z., G.G., A.M.P., E.F.V. and L.I.; Supervision, E.F.V and L.I.

Declaration of interest

The authors declare no competing interests

Figures

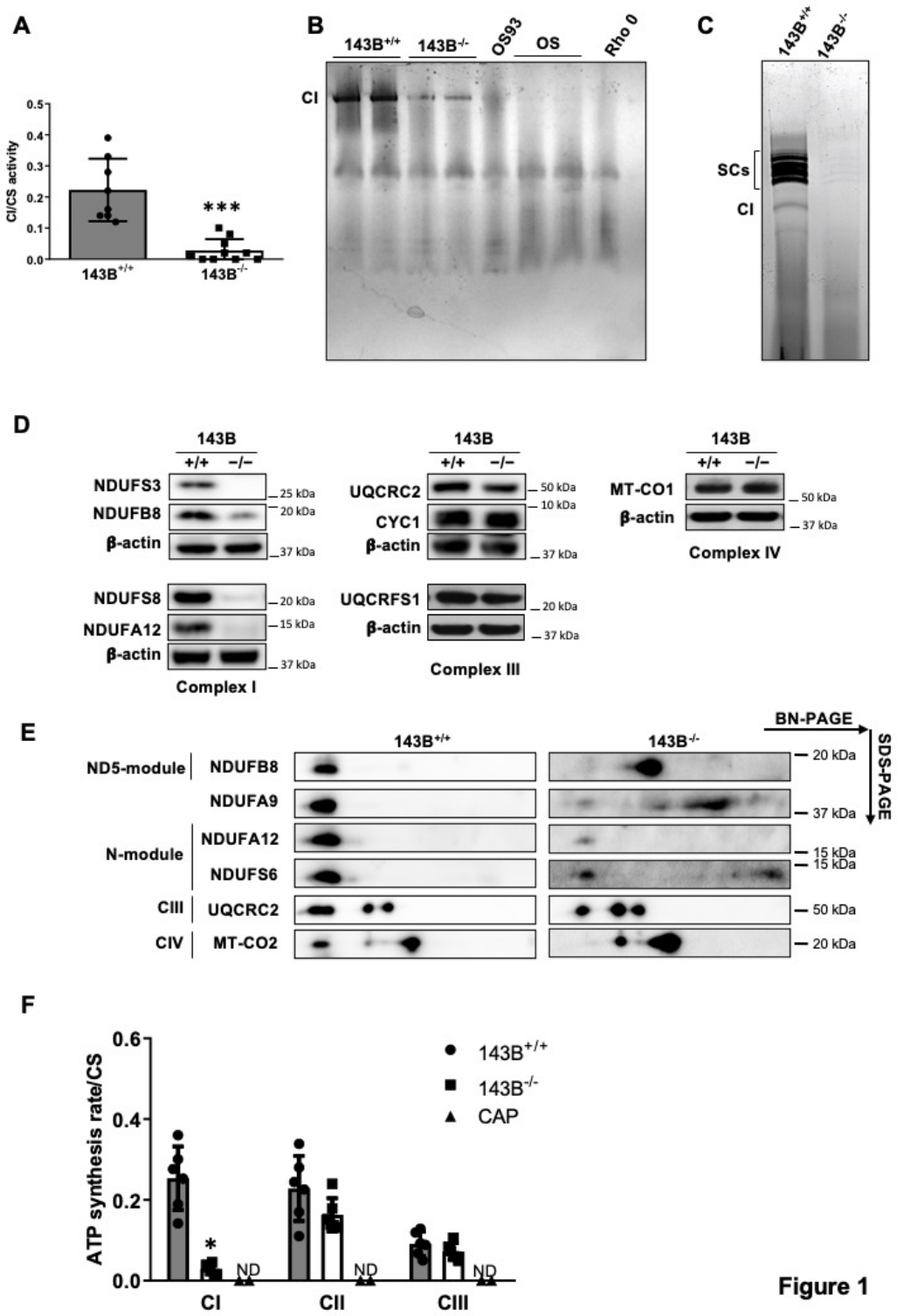

Figure 1. A residual, but still detectable, fully assembled and functional respiratory CI is present in constitutive *NDUFS3* KO cells. A) Spectrophotometric kinetic measurements of complex I (CI) activity normalized to citrate synthase (CS). Data in the graph are represented as mean ± SD (n = 9 biological replicates for $143B^{-/-}$ and n = 10 for $143B^{+/+}$). ***p = 0.0009 according

to unpaired Student's t-test. **B**) Complex I in-gel activity (CI-IGA) assay using MTT as the substrate, of $143B^{+/+}$, $143B^{-/-}$, OS93, OS and Rho0 samples solubilized with 1.6 mg DDM/mg protein and separated by High-Resolution Clear Native PAGE (hrCNE) **C**) CI-IGA assay of $143B^{+/+}$ and $143B^{-/-}$ samples, using NTB as the substrate and solubilized with 4 mg digitonin/mg protein and separated by BN-PAGE. SCs include $CI+III_2$ and respirasomes ($I+III_2+IV_{1-n}$). **D**) Immunodetection of CI, CIII and CIV subunits on Western blots of whole-cell lysates from $143B^{+/+}$ and $143B^{-/-}$ cells lines resolved by SDS-PAGE. β-actin was used as the loading control for each blot. **E**) Immunodetection of CI, CIII and CIV subunits on Western blots of mitochondrial enriched fraction from $143B^{+/+}$ and $143B^{-/-}$ cell lines solubilized with 4 mg digitonin/mg protein and resolved by 2D BN-PAGE. All the subunits were immunodetected on the same blot. **F**) CI-, CII- and CIII-driven ATP synthesis rates for $143B^{+/+}$ and $143B^{-/-}$ either treated or not with 50 µg/mL Chloramphenicol (CAP). Specific ATP synthesis rates (nmol/min*mg) were normalized to CS specific activity. The values represented in the graph are mean ± SD. *$p < 0.0001$; multiple t tests of Two-way ANOVA, Holm-Sidak method, with alpha=5.000%. ND: not detected.

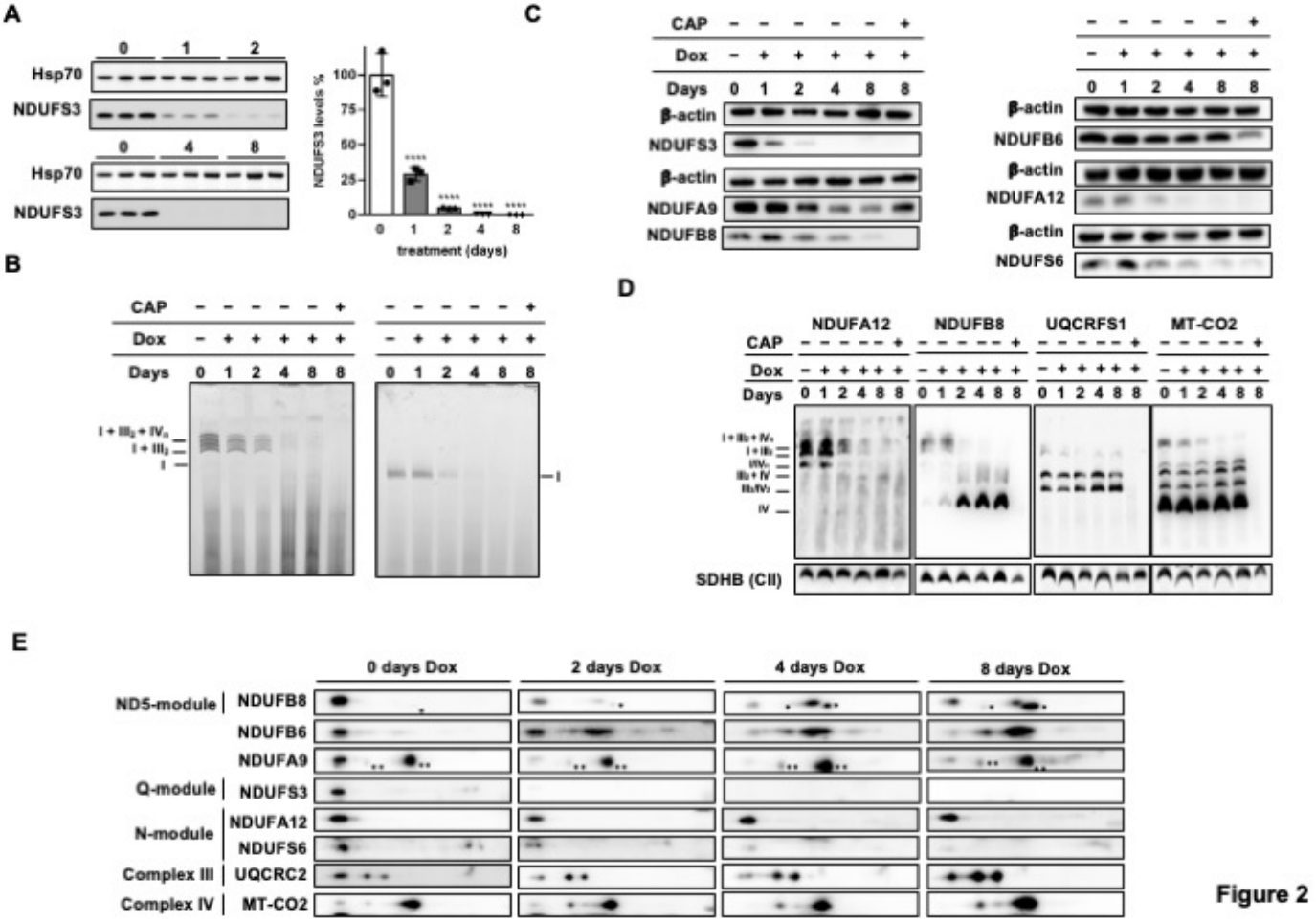

Figure 2

Figure 2. Persistence of functional respiratory CI during repression of *NDUFS3*. A) Immunodetection of NDUFS3 on Western blots of whole-cell lysates from 143B$^{-/-\ NDUFS3}$ cells treated with 100 ng/mL doxycycline (Dox) for 0 (untreated), 1, 2, 4 and 8 days (n = 3 biological replicates). NDUFS3 band signal intensities were quantified by densitometry and normalized to the signal of Hsp70. The mean values of the treated cells were referred to those of untreated control set to 100%. Data represented on the graph are mean ± SD. ****$p < 0.0001$ treated vs. untreated; ANOVA with Sidak's multiple comparisons test. **B**) Immunodetection of CI subunits on Western blots of 143B$^{-/-NDUFS3}$ cells, treated either with 100 ng/mL for 0 (untreated), 1, 2, 4 and 8 days or simultaneously with 100 ng/mL Dox and 50 µg/mL CAP for 8 days, resolved by SDS-PAGE. β-actin was used as the loading control. **C**) CI-IGA, using NTB as the substrate, of enriched mitochondrial fraction from repressed 143B$^{-/-NDUFS3}$, solubilized either with 4 mg digitonin/ mg protein or 1.6 mg/DDM/ mg protein and separated by BN-PAGE. SCs include CI+III_2 and respirasomes (I+III_2+IV_{1-n}). **D**) Immunodetection of CI subunits NDUFA12 (N-module) and NDUFB8 (ND5-module), CIII subunit UQCRFS1 and CIV subunit MT-CO2, in Western blots of enriched mitochondrial fraction from 143B$^{-/-NDUFS3}$ cells treated as in B solubilized either with 4 mg digitonin/ mg protein or 1.6 mg DDM/ mg protein and separated by BN-PAGE. SCs include CI+III_2

and respirasomes ($I+III_2+IV_{1-n}$). SDHB (CII) was used as the loading control. **E**) Immunodetection of CI, CIII and CIV subunits on Western blots of mitochondrial enriched fraction from $143B^{-/-}$ ^{NDUFS3} cells treated with 100 ng/mL Dox for 0 (untreated), 2, 4 and 8 days, solubilized with 4 mg digitonin/mg protein and resolved by 2D BN-PAGE. All the subunits were immunodetected on the same blot. One asterisk (*) indicates a not specific signal derived from an anti-NDUFA8 antibody with which the membrane was previously incubated. Two asterisks (**) indicate a signal derived from antibody anti-MT-CO1.

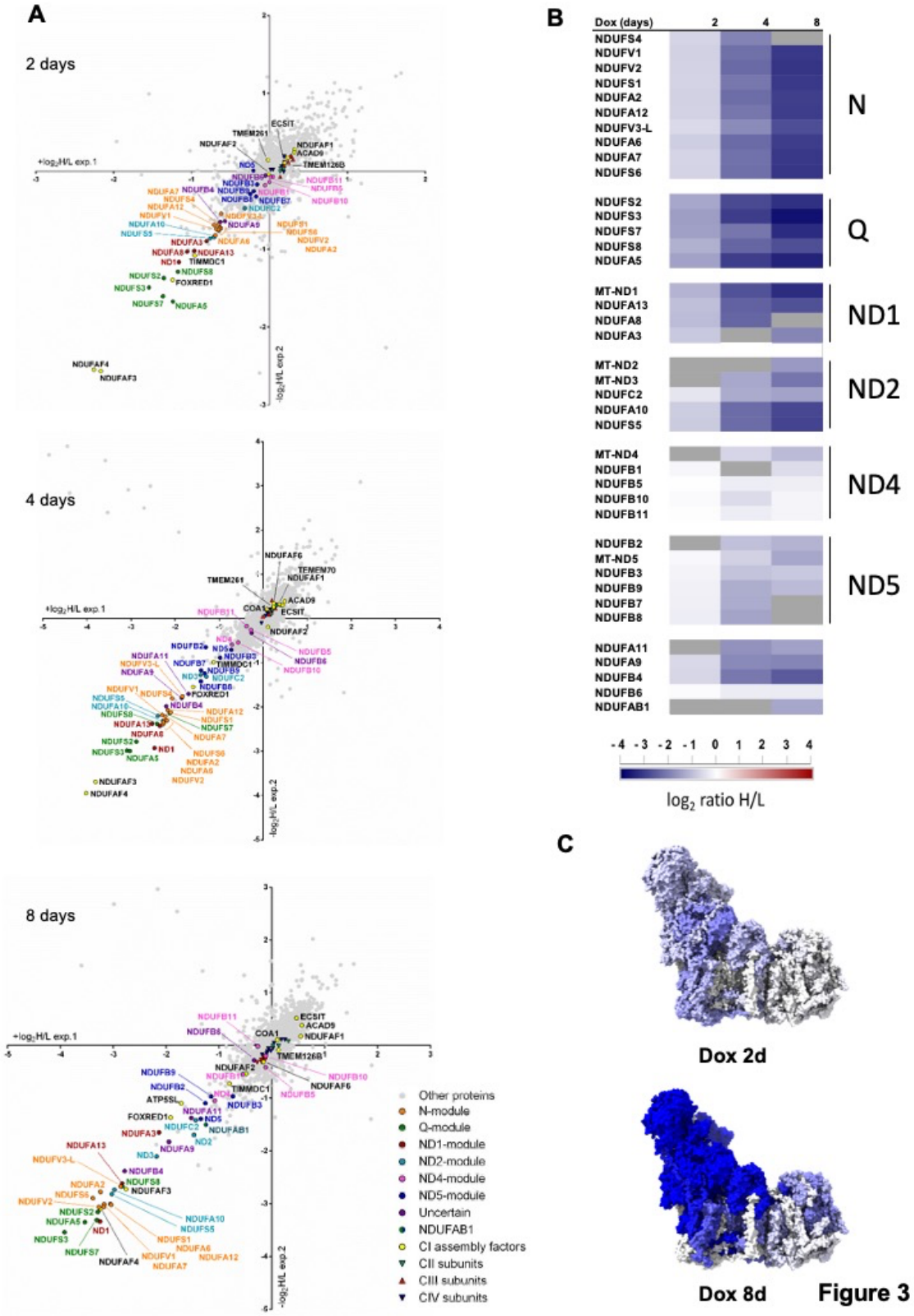

Figure 3

Figure 3. Progressive loss of NDUFS3 reveals the modular dynamics of CI disassembly. **A**) Scatter plots generated from the MS analysis of two reciprocal duplicate SILAC experiments

(experiments 1 and 2) of comparing untreated 143B$^{-/-NDUFS3}$ with cells treated with 100 ng/mL Dox for 2, 4 or 8 days. Mitochondrial enriched fractions for each reciprocal duplicate were obtained and analyzed by MS. The values of the logarithmic fold change (log_2H/L) for each protein in experiment 1 (exp.1; Light untreated, Heavy Dox treated) are represented in the x-axis. The logarithmic fold change values (-log_2H/L) derived from experiment 2 (exp.2; Heavy untreated, Light Dox treated) are represented in the y-axis. Each point represents a specific protein. CI subunits and assembly factors are highlighted; CI subunits assigned to the same module are represented with the same color. The group termed "uncertain" includes the subunits with a still unclear assignment (6). Proteins showing statistically significant changes are also indicated in the graphs. **B**) Heatmap generated from the mean of the two-reciprocal duplicate SILAC experiments for the detected CI subunits at each of Dox treatment point (2, 4 and 8 days). Grey: not detected either in one or both of the duplicate experiments. **C**) CI structural subunit relative protein abundance changes induced by repression of NDUFS3 after 2 and 8 days of Dox treatment depicted on the structure of active mouse CI (PDB: 6G2J) (5) using ChimeraX v1.1 (61).

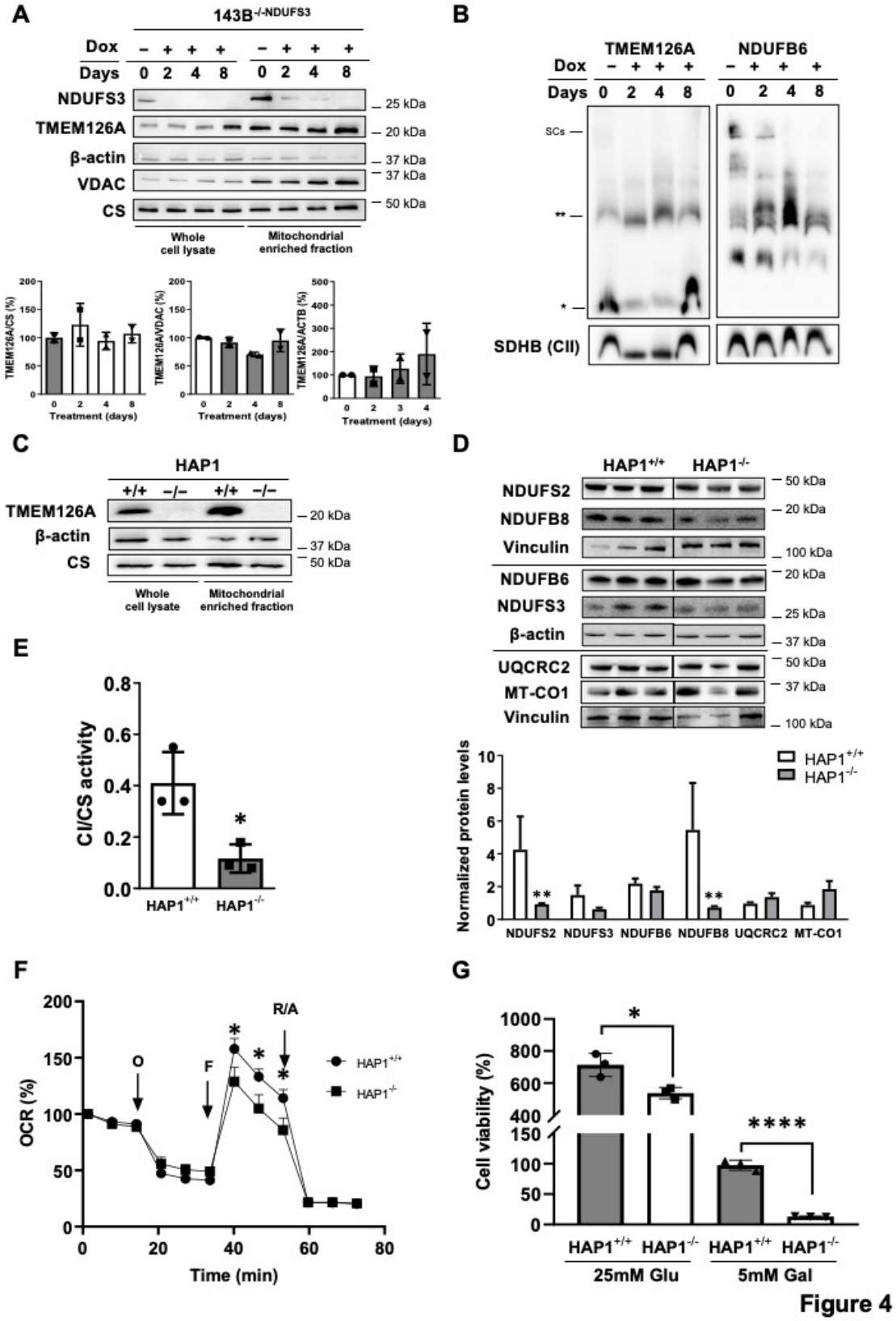

Figure 4. TMEM126A is required for a complete biogenesis of respiratory CI. A) Immunodetection of TMEM126A and NDUFS3 on Western blots of whole-cell lysates and

mitochondrial enriched fractions from 143B$^{-/-\ NDUFS3}$ cells treated with 100 ng/mL doxycycline (Dox) for 0 (untreated), 1, 2, 4 and 8 days (n = 2). TMEM126A band signal intensities were quantified by densitometry and normalized to the signal of either vinculin for whole cell lysates and citrate synthase (CS) or voltage-dependent anion channel (VDAC) for mitochondrial enriched fractions. The mean values of the treated cells were referred to those of untreated control set to 100%. Data were represented on the graph are mean ± SD. One-way ANOVA and one-sample t-test were used for statistics. **B**) Immunodetection of TMEM126A and NDUFB6 (ND4-module), in Western blots of enriched mitochondrial fraction from 143B$^{-/-NDUFS3}$ cells treated as in A solubilized 4 mg digitonin/ mg protein and separated by BN-PAGE. Two asterisks (**) indicate a subassembly containing TMEM126A and co-migrating with NDUFB6 subassembly; One asterisk (*) indicates a lower molecular weight subassembly with positive staining for TMEM126A. SDHA (CII) was used as the loading control. **C**) Immunodetection of TMEM126A on Western blots of whole-cell lysates and mitochondrial enriched fractions from HAP1$^{+/+}$ and HAP1$^{-/-}$ cells. β-actin and CS were used as the loading controls. **D**) Immunodetection of CI, CIII and CIV subunits on Western blots of whole-cell lysates from HAP1$^{+/+}$ and HAP1$^{-/-}$ cells lines (n = 3-4 biological replicates) resolved by SDS-PAGE. β-actin or vinculin were used as the loading controls. Band signal intensities were quantified by densitometry and normalized to the signal of the relative loading control. The mean values of the treated cells were referred to those of untreated control set to 100%. Data were represented on the graph are mean ± SD. **$p < 0.01$ according to unpaired Multiple t-test, Holm-Sidak method, with alpha = 0.05. **E**) Spectrophotometric kinetic measurements of CI activity normalized to citrate synthase (CS). Data in the graph are represented as mean ± SD (n = 3 biological replicates) ***$p = 0.0189$ according to unpaired Student's t-test. **F**)
Oxygen consumption rate (OCR) profile in HAP1$^{+/+}$ and HAP1$^{-/-}$ cells. Measurements of OCR were performed upon injection of 1 μM oligomycin (O), 0.25 μM FCCP (F), 1 μM rotenone plus antimycin A (R/A) diluted in Seahorse medium, pH 7.4. Data are expressed as percentage referred to initial basal respiration and normalized on SRB absorbance and showen as mean+SEM of n = 4 independent biological replicates, ∗$p<0.01$ according to Multiple t-test Holm-Sidak method, with alpha = 0.05. **F**) HAP1$^{+/+}$ and HAP1$^{-/-}$ cell viability determined by sulforhodamine B (SRB) assay after 72 hours of incubation with either 25 mM glucose or glucose-free medium containing 5mM galactose. Data are mean ± SD of n = 4 independent biological replicates, ∗$p= 0.0197$ and ***$p<0.0001$ according to two-tailed unpaired Student's t-test.

References

1. J. Hirst, Mitochondrial Complex I. *Annual Review of Biochemistry* **82**, 551–575 (2013).

2. L. A. Sazanov, A giant molecular proton pump: Structure and mechanism of respiratory complex I. *Nature Reviews Molecular Cell Biology* **16**, 375–388 (2015).

3. R. Baradaran, J. M. Berrisford, G. S. Minhas, L. A. Sazanov, Crystal structure of the entire respiratory complex i. *Nature* **494**, 443–448 (2013).

4. J. Zhu, K. R. Vinothkumar, J. Hirst, Structure of mammalian respiratory complex I (2016) https:/doi.org/10.1038/nature19095.

5. A. N. A. Agip, *et al.*, Cryo-em structures of complex i from mouse heart mitochondria in two biochemically defined states. *Nature Structural and Molecular Biology* **25** (2018).

6. D. A. Stroud, *et al.*, Accessory subunits are integral for assembly and function of human mitochondrial complex i. *Nature* **538**, 123–126 (2016).

7. K. R. Vinothkumar, J. Zhu, J. Hirst, Architecture of mammalian respiratory complex I. *Nature* **515**, 80–84 (2014).

8. S. Guerrero-Castillo, *et al.*, The Assembly Pathway of Mitochondrial Respiratory Chain Complex I. *Cell Metabolism* **25**, 128–139 (2017).

9. L. Sánchez-Caballero, S. Guerrero-Castillo, L. Nijtmans, Unraveling the complexity of mitochondrial complex i assembly: A dynamic process. *Biochimica et Biophysica Acta - Bioenergetics* **1857**, 980–990 (2016).

10. T. Friedrich, D. Scheide, The respiratory complex I of bacteria, archaea and eukarya and its module common with membrane-bound multisubunit hydrogenases. *FEBS Letters* **479**, 1–5 (2000).

11. V. K. Moparthi, C. Hägerhäll, The evolution of respiratory chain complex i from a smaller last common ancestor consisting of 11 protein subunits. *Journal of Molecular Evolution* **72**, 484–497 (2011).

12. L. E. Formosa, M. G. Dibley, D. A. Stroud, M. T. Ryan, Building a complex complex: Assembly of mitochondrial respiratory chain complex I. *Seminars in Cell and Developmental Biology* **76**, 154–162 (2018).

13. R. Acin-Perez, J. A. Enriquez, The function of the respiratory supercomplexes: The plasticity model. *Biochimica et Biophysica Acta (BBA) - Bioenergetics* **1837**, 444–450 (2014).

14. D. Milenkovic, J. N. Blaza, N.-G. Larsson, J. Hirst, The Enigma of the Respiratory Chain Supercomplex. *Cell Metabolism* **25**, 765–776 (2017).

15. T. Lobo-Jarne, C. Ugalde, Respiratory chain supercomplexes: Structures, function and biogenesis. *Seminars in Cell & Developmental Biology* **76**, 179–190 (2018).

16. R. Acín-Pérez, P. Fernández-Silva, M. L. Peleato, A. Pérez-Martos, J. A. Enriquez, Respiratory Active Mitochondrial Supercomplexes. *Molecular Cell* **32**, 529–539 (2008).

17. D. Moreno-Lastres, *et al.*, Mitochondrial complex I plays an essential role in human respirasome assembly. *Cell Metabolism* **15**, 324–335 (2012).

18. M. Protasoni, *et al.*, Respiratory supercomplexes act as a platform for complex III -mediated maturation of human mitochondrial complexes I and IV. *The EMBO Journal* **39** (2020).

19. R. O. Vogel, *et al.*, Identification of mitochondrial complex I assembly intermediates by tracing tagged NDUFS3 demonstrates the entry point of mitochondrial subunits. *Journal of Biological Chemistry* **282**, 7582–7590 (2007).

20. C. E. J. Dieteren, *et al.*, Subunit-specific incorporation efficiency and kinetics in mitochondrial complex i homeostasis. *Journal of Biological Chemistry* **287**, 41851–41860 (2012).

21. P. Bénit, *et al.*, Mutant NDUFS3 subunit of mitochondrial complex I causes Leigh syndrome. *Journal of Medical Genetics* **41**, 14–17 (2004).

22. T. M. Jaokar, D. P. Patil, Y. S. Shouche, S. M. Gaikwad, C. G. Suresh, Human mitochondrial NDUFS3 protein bearing Leigh syndrome mutation is more prone to aggregation than its wild-type. *Biochimie* **95**, 2392–2403 (2013).

23. X. Lou, *et al.*, A Novel NDUFS3 mutation in a Chinese patient with severe Leigh syndrome. *Journal of Human Genetics* **63**, 1269–1272 (2018).

24. H. Pagniez-Mammeri, *et al.*, Rapid screening for nuclear genes mutations in isolated respiratory chain complex I defects. *Molecular Genetics and Metabolism* **96**, 196–200 (2009).

25. C. V Pereira, *et al.*, Myopathy reversion in mice after restauration of mitochondrial complex I. *EMBO Molecular Medicine* **12** (2020).

26. I. Kurelac, *et al.*, Inducing cancer indolence by targeting mitochondrial Complex I is potentiated by blocking macrophage-mediated adaptive responses. *Nature Communications* **10** (2019).

27. L. Iommarini, *et al.*, Unravelling the effects of the mutation m.3571insC/MT-ND1 on respiratory complexes structural organization. *International Journal of Molecular Sciences* **19**, 764 (2018).

28. E. Fassone, *et al.*, FOXRED1, encoding an FAD-dependent oxidoreductase complex-I-specific molecular chaperone, is mutated in infantile-onset mitochondrial encephalopathy. *Human Molecular Genetics* **19**, 4837–4847 (2010).

29. L. E. Formosa, *et al.*, Characterization of mitochondrial FOXRED1 in the assembly of respiratory chain complex I. *Human Molecular Genetics* **24**, 2952–2965 (2015).

30. D. M. Elurbe, M. A. Huynen, The origin of the supernumerary subunits and assembly factors of complex I: A treasure trove of pathway evolution ☆ (2016) https:/doi.org/10.1016/j.bbabio.2016.03.027.

31. D. Ghezzi, M. Zeviani, Human diseases associated with defects in assembly of OXPHOS complexes. *Essays In Biochemistry* **62**, 271–286 (2018).

32. R. Acín-Pérez, *et al.*, Respiratory complex III is required to maintain complex I in mammalian mitochondria. *Molecular Cell* **13**, 805–815 (2004).

33. O. Barel, *et al.*, Mitochondrial Complex III Deficiency Associated with a Homozygous Mutation in UQCRQ. *American Journal of Human Genetics* **82**, 1211–1216 (2008).

34. V. Carossa, *et al.*, A novel in-frame 18-bp microdeletion in MT-CYB causes a multisystem disorder with prominent exercise intolerance. *Hum. Mutat.* **35**, 954–958 (2014).

35. R. G. Feichtinger, *et al.*, Combined Respiratory Chain Deficiency and UQCC2 Mutations in Neonatal Encephalomyopathy: Defective Supercomplex Assembly in Complex III Deficiencies. *Oxidative Medicine and Cellular Longevity* **2017**, 11–11 (2017).

36. E. Lamantea, *et al.*, A novel nonsense mutation (Q352X) in the mitochondrial cytochrome b gene associated with a combined deficiency of complexes I and III. *Neuromuscular Disorders* **12**, 49–52 (2002).

37. E. J. Tucker, *et al.*, Mutations in the UQCC1-Interacting Protein, UQCC2, Cause Human Complex III Deficiency Associated with Perturbed Cytochrome b Protein Expression. *PLoS Genetics* **9** (2013).

38. F. Diaz, H. Fukui, S. Garcia, C. T. Moraes, Cytochrome c Oxidase Is Required for the Assembly/Stability of Respiratory Complex I in Mouse Fibroblasts. *Molecular and Cellular Biology* **26**, 4872–4881 (2006).

39. T. Lobo-Jarne, *et al.*, Multiple pathways coordinate assembly of human mitochondrial complex IV and stabilization of respiratory supercomplexes. *International Journal of STD and AIDS* **39**, e103912 (2020).

40. D. Moreno-Lastres, *et al.*, Mitochondrial Complex I Plays an Essential Role in Human Respirasome Assembly. *Cell Metabolism* **15**, 324–335 (2012).

41. A. Timón-Gómez, J. Garlich, R. A. Stuart, C. Ugalde, A. Barrientos, Distinct Roles of Mitochondrial HIGD1A and HIGD2A in Respiratory Complex and Supercomplex Biogenesis. *Cell Reports* **31**, 107607 (2020).

42. A. Guarás, *et al.*, The CoQH2/CoQ Ratio Serves as a Sensor of Respiratory Chain Efficiency. *Cell Rep* **15**, 197–209 (2016).

43. L. E. Formosa, *et al.*, Dissecting the Roles of Mitochondrial Complex I Intermediate Assembly Complex Factors in the Biogenesis of Complex I. *Cell Rep* **31**, 107541 (2020).

44. H. Heide, *et al.*, Complexome profiling identifies TMEM126B as a component of the mitochondrial complex I assembly complex. *Cell Metab.* **16**, 538–549 (2012).

45. J. Désir, *et al.*, TMEM126A mutation in a Moroccan family with autosomal recessive optic atrophy. *Molecular vision* **18**, 1849–57 (2012).

46. S. Hanein, *et al.*, TMEM126A, Encoding a Mitochondrial Protein, Is Mutated in Autosomal-Recessive Nonsyndromic Optic Atrophy. *American Journal of Human Genetics* **84**, 493–498 (2009).

47. C. La Morgia, *et al.*, First TMEM126A missense mutation in an Italian proband with optic atrophy and deafness. *Neurology: Genetics* **5** (2019).

48. E. Meyer, *et al.*, Nonsense mutation in TMEM126A causing autosomal recessive optic atrophy and auditory neuropathy. *Molecular Vision* **16**, 650–664 (2010).

49. H.-F. Sun, *et al.*, Loss of TMEM126A promotes extracellular matrix remodeling, epithelial-to-mesenchymal transition, and breast cancer metastasis by regulating mitochondrial retrograde signaling. *Cancer Lett.* **440–441**, 189–201 (2019).

50. A. M. Porcelli, *et al.*, The genetic and metabolic signature of oncocytic transformation implicates HIF1α destabilization. *Human Molecular Genetics* **19**, 1019–1032 (2010).

51. G. Gasparre, *et al.*, A mutation threshold distinguishes the antitumorigenic effects of the mitochondrial gene MTND1, an Oncojanus function. *Cancer Research* **71**, 6220–6229 (2011).

52. S. E. Ong, *et al.*, Stable isotope labeling by amino acids in cell culture, SILAC, as a simple and accurate approach to expression proteomics. *Molecular & cellular proteomics : MCP* **1**, 376–386 (2002).

53. L. G. J. Nijtmans, N. S. Henderson, I. J. Holt, Blue Native electrophoresis to study mitochondrial and other protein complexes. *Methods* **26**, 327–334 (2002).

54. I. Wittig, H. P. Braun, H. Schägger, Blue native PAGE. *Nature Protocols* **1**, 418–428 (2006).

55. A. Ghelli, *et al.*, The cytochrome b p.278Y>C mutation causative of a multisystem disorder enhances superoxide production and alters supramolecular interactions of respiratory chain complexes. *Human Molecular Genetics* **22**, 2141–2151 (2013).

56. B. Andrews, J. Carroll, S. Ding, I. M. Fearnley, J. E. Walker, Assembly factors for the membrane arm of human complex i. *Proceedings of the National Academy of Sciences of the United States of America* **110**, 18934–18939 (2013).

57. J. Cox, M. Mann, MaxQuant enables high peptide identification rates, individualized p.p.b.-range mass accuracies and proteome-wide protein quantification. *Nature Biotechnology* **26**, 1367–1372 (2008).

58. J. Cox, *et al.*, Andromeda: A peptide search engine integrated into the MaxQuant environment. *Journal of Proteome Research* **10**, 1794–1805 (2011).

59. J. Cox, M. Mann, Quantitative, High-Resolution Proteomics for Data-Driven Systems Biology. *Annual Review of Biochemistry* **80**, 273–299 (2011).

60. S. Tyanova, *et al.*, The Perseus computational platform for comprehensive analysis of (prote)omics data. *Nature Methods* **13**, 731–740 (2016).

61. T. D. Goddard, *et al.*, UCSF ChimeraX: Meeting modern challenges in visualization and analysis. *Protein Sci.* **27**, 14–25 (2018).